J. Fluid Mech. (1993), *vol.* 246, *pp.* 343–360

Temperature dependence of rotational relaxation in shock waves of nitrogen

By I. D. BOYD†
Eloret Institute, NASA Ames Research Center, MS 230-2, CA 94035, USA

(Received 6 January 1992 and in revised form 28 July 1992)

Computations are presented for one-dimensional shockwaves of diatomic nitrogen. The direct simulation Monte Carlo method (DSMC) is employed. A model which allows the use of the Sutherland viscosity model in the DSMC technique is further developed to include the modelling of rotational relaxation. This is achieved by employing a temperature-dependent expression for the rotational collision number to simulate the rate of relaxation, in contrast to earlier DSMC studies which employed a constant value for the collision number. The behaviour of the new model is first considered for rotational relaxation in a heat bath. Comparison is made with the more traditional DSMC collision model termed the variable hard sphere (VHS) model in which the viscosity has a fixed temperature exponent. These two models are then applied to a number of shock-wave cases for which experimental data exist. These have Mach numbers ranging from 1.5 to 26, yet the enthalpies involved are sufficiently low to allow omission of vibrational relaxation. It is found that both the VHS and Sutherland viscosity models give excellent agreement with the experimental data for shock-wave thickness, and for profiles of density, rotational temperature, and velocity. The most significant finding of the study is that the reciprocal shock thickness varies with the upstream temperature condition. This variation is observed in the experimental data, and is simulated numerically by employing the temperature-dependent expression for the rotational collision number.

1. Introduction

The one-dimensional shock wave of a diatomic gas is a flow which has been investigated widely using both experimental (Alsmeyer 1976; Robben & Talbot 1966; Smith 1972; Butefisch & Vennemann 1974) and computational (Alsmeyer 1976; MacPherson 1971; Melville 1972; Boyd 1990*b*) techniques. For low-enthalpy upstream conditions, in which vibrational and chemical relaxation phenomena are insignificant, the problem has been viewed generally as being non-dimensional for a given Mach number, with length normalized by the upstream mean-free path. The present numerical investigation also focuses on strong shock waves of nitrogen. Consideration is given to cases for which experimental measurements exist. Using the electron-beam technique, shock thicknesses (Alsmeyer 1976; Robben & Talbot 1966), density profiles (Alsmeyer 1976; Robben & Talbot 1966; Smith 1972), and rotational temperature profiles (Robben & Talbot 1966; Smith 1972) have been measured. Using a time-of-flight technique, the velocity profile has been measured (Butefisch & Vennemann 1974). The upstream flow conditions in these experiments provided a Mach number range of about 1.5 to 26; however, the upstream

† Present address: School of Mechanical and Aerospace Engineering, Cornell University, Ithaca, NY 14853, USA.

temperature was not the same for each investigation. In the study of Alsmeyer (1976), a shock tube was employed giving an initial temperature of about 300 K. In other experiments (Robben & Talbot 1966; Smith 1972; Butefisch & Vennemann 1974), a shock holder was inserted in an expansion jet giving in some cases very low upstream temperatures of 30 K or less. Comparison of these experimental data sets reveals significant differences. Specifically, the shocks measured by Alsmeyer were thicker than those observed by the others. It is the purpose of the present numerical investigation to discover whether these differences can be explained in terms of a dependence of the shock-wave profiles on the absolute value of the upstream temperature.

The computational technique employed is the direct simulation Monte Carlo method (DSMC) of Bird (1976). The method models the flow with a set of model particles. The motions and collisions of these particles are followed through physical space. The method is a popular technique in the analysis of flows for which the characteristic length is of the order of a mean-free path. Under such conditions, the Navier–Stokes equations are invalid owing to the failure of the linear constitutive relations for viscous shear stress and heat conductivity. Such flows include strong shock waves, and the field of rarefied gas dynamics in general. This technique has been applied to model rotational relaxation of nitrogen in shock waves. MacPherson (1971) performed DSMC computations using a detailed collision dynamics approach, while Melville (1972) introduced the idea of the loaded sphere into the DSMC technique. These concepts have been abandoned in favour of less detailed, more numerically efficient, phenomenological models which appear capable of capturing the important physical behaviour (Alsmeyer 1976; Boyd 1990*b*). For the calculations presented by Alsmeyer, the collision model assumed a viscosity law with a fixed temperature-exponent in which the intermolecular potential is described by a simple inverse-power law of repulsion. The rate of rotational relaxation was modelled with a constant rotational collision number. These assumptions provide solutions which are independent of temperature, and good agreement was obtained with the experimental data also reported by Alsmeyer. Neither of those data sets can, however, be reconciled with the other experimental results. In the present study, theoretical developments are reported which permit the use of the Sutherland viscosity law in the DSMC method for simulating a diatomic gas. This model adds an attractive portion to the hard-sphere intermolecular potential. The strength of attraction is proportional to a characteristic temperature of the molecule. In the present study, the rate of rotational relaxation is modelled with the energy-dependent collision number developed by Boyd (1990*b*). Both of these theoretical models place a dependence of the solutions generated on the initial upstream temperature.

The paper proceeds by describing the general method for computing rotational relaxation with the DSMC technique. The model development for employing the Sutherland viscosity law for a rotationally relaxing gas is then described. Test calculations in a heat bath are presented in order to characterize the features of the new rotational relaxation model. Finally, direct comparison is made between computations and many of the experimental results reported by Alsmeyer, Robben & Talbot, Smith, and Butefisch & Vennemann.

2. Simulation of rotational relaxation in the DSMC method

Generally, in the DSMC technique, the rotational energy distribution is treated classically, with a continuous distribution. For nitrogen, this is a reasonable assumption as the characteristic temperature for rotation is just 2.878 K. The exchange of energy between the rotational and translational modes of a gas involves the modelling of two distinct phenomena: the mechanics of energy exchange, and the rate of energy exchange. This section describes how to simulate these two aspects of rotational relaxation using the variable hard sphere (VHS) collision model of Bird (1981).

The VHS model is based on a fixed temperature exponent law in which the viscosity coefficient is given by

$$\mu_{\mathrm{VHS}} = \mu_{\mathrm{ref}}(T/T_{\mathrm{ref}})^{\omega}. \tag{1}$$

This behaviour is reproduced at the collisional level by the following collision cross-section:

$$\sigma_{\mathrm{VHS}} = \sigma_{\mathrm{ref}} g^{1-2\omega}, \tag{2}$$

where g is the relative collision velocity. In the DSMC method, the collision probability is proportional to the product of the cross-section in (2) and the relative velocity. The viscosity behaviour modelled by the VHS approach is identical to the more familiar inverse-power collision model. The only difference is that the VHS model treats the mechanical interaction between the colliding bodies as if they were hard spheres for all values of ω.

The simulation of energy exchange is handled using the Borgnakke–Larsen (1975) approach. In this method, the total energy, given by the sum of the translational collision energy and the rotational energies of the colliding bodies, is redistributed statistically by sampling the appropriate equilibrium distribution function. The distribution for the relative velocity of colliding particles in a VHS gas is filtered by the collision cross-section, (2), and may be expressed as

$$f_{\mathrm{VHS}}\left(\frac{E_{\mathrm{t}}}{kT}\right) = \frac{1}{\Gamma(\frac{5}{2}-\omega)}\left(\frac{E_{\mathrm{t}}}{kT}\right)^{\frac{3}{2}-\omega}\exp\left(\frac{-E_{\mathrm{t}}}{kT}\right), \tag{3}$$

where $E_{\mathrm{t}} = \frac{1}{2}m_{\mathrm{r}}g^2$ is the translational collision energy, and m_{r} is the reduced mass of the colliding particles. This distribution may be combined with that for the rotational energy of the colliding particles to give the following distribution for the ratio of the translational collision energy to the total energy of the collision, E_{c}:

$$f_{\mathrm{VHS}}\left(\frac{E_{\mathrm{t}}}{E_{\mathrm{c}}}\right) = \left[\frac{\frac{1}{2}+\zeta-\omega}{\frac{3}{2}-\omega}\frac{E_{\mathrm{t}}}{E_{\mathrm{c}}}\right]^{\frac{3}{2}-\omega}\left[\frac{\frac{1}{2}+\zeta-\omega}{\zeta-1}\left(1-\frac{E_{\mathrm{t}}}{E_{\mathrm{c}}}\right)\right]^{\zeta-1}, \tag{4}$$

where ζ is the average number of rotational degrees of freedom of the colliding particles. This function is sampled statistically to determine the post-collision partitioning of the translational and rotational energies. A further distribution function is employed to partition the total rotational energy between the colliding particles. The translational collision energy is partitioned using hard-sphere collision mechanics which conserve linear momentum and energy.

Simulation of the rate of rotational relaxation in the DSMC technique has been studied by Boyd (1990*a*, *b*). The following result for the rotational collision number, Z_{r}, was developed by Parker (1959) using classical mechanics:

$$Z_{\mathrm{r}} = \frac{Z_{\infty}}{1+\frac{1}{2}\pi^{\frac{3}{2}}(T^*/T)^{\frac{1}{2}}+(\frac{1}{4}\pi^2+2)\,T^*/T}, \tag{5}$$

where T^* is the characteristic temperature of the intermolecular potential, and Z_∞ is the limiting value. The form given in (5) includes the correction to Parker's formula noted by Brau & Jonkman (1970). For each collision simulated in the DSMC method, the probability of rotational relaxation is given simply by the reciprocal of the collision number. To reproduce Parker's result in the particle simulation, a probability must be formulated. When integrated over the equilibrium distribution for the total collision energy, E_c, this probability should provide the temperature dependence of (5). For the VHS model, the appropriate distribution is

$$f_{\mathrm{VHS}}\left(\frac{E_c}{kT}\right) = \frac{1}{\Gamma(\zeta+\frac{5}{2}-\omega)}\left(\frac{E_c}{kT}\right)^{\zeta+\frac{3}{2}-\omega}\exp\left(\frac{-E_c}{kT}\right). \tag{6}$$

With this distribution, Boyd (1990*b*) showed that the necessary energy exchange probability is given by

$$\phi_{\mathrm{VHS}} Z_\infty = 1+\frac{\Gamma(\zeta+\frac{5}{2}-\omega)}{\Gamma(\zeta+2-\omega)}\left(\frac{kT^*}{E_c}\right)^{\frac{1}{2}}\frac{\pi^{\frac{3}{2}}}{2}+\frac{\Gamma(\zeta+\frac{5}{2}-\omega)}{\Gamma(\zeta+\frac{3}{2}-\omega)}\left(\frac{kT^*}{E_c}\right)\left(\frac{\pi^2}{4}+2\right). \tag{7}$$

The procedure employed to simulate energy relaxation in a particle method affects the rate of relaxation. Therefore a correction must be applied to (7) to produce a collision number which is consistent with those defined for continuum or experimental rate data. The correction for the VHS model has been determined analytically by Lumpkin, Haas & Boyd (1991) and is given by

$$(Z_r^{\mathrm{part}})_{\mathrm{VHS}} = Z_r^{\mathrm{cont}}\frac{5-2\omega}{5-2\omega+2\zeta}. \tag{8}$$

The VHS models described above for the particle simulation of the mechanics and rate of rotational relaxation have been applied quite successfully under conditions of high temperature (Boyd 1992). In the following section, the corresponding models will be developed for the Sutherland model which is more appropriate for application to low-temperature flows.

3. Simulation of rotational relaxation with the Sutherland model

The Sutherland viscosity law has the following form:

$$\mu_{\mathrm{Suth}} = \mu_{\mathrm{ref}}\left(\frac{T}{T_{\mathrm{ref}}}\right)^{\frac{3}{2}}\frac{T_{\mathrm{ref}}+T^*}{T+T^*}, \tag{9}$$

where T^* is the same characteristic temperature introduced in (5). The variation with temperature of the VHS and Sutherland models are compared in figure 1 with the detailed viscosity computations reported by Jacobsen *et al.* (1973). The appropriate reference quantities employed in (1) and (9) are $\mu_{\mathrm{ref}} = 1.63\times10^{-5}$ N m^{-1} s^{-1} and $T_{\mathrm{ref}} = 273$ K. While there are some differences between these viscosity profiles (mainly at the very low temperatures) it is clear that both the VHS and Sutherland models correspond reasonably with the detailed calculations.

It has been shown by Kuscer (1990) that a collision cross-section which simulates the Sutherland viscosity law at the molecular level is given by

$$\sigma_{\mathrm{Suth}} = \sigma_\infty\left(1+\frac{12kT^*}{mg^2}\right), \tag{10}$$

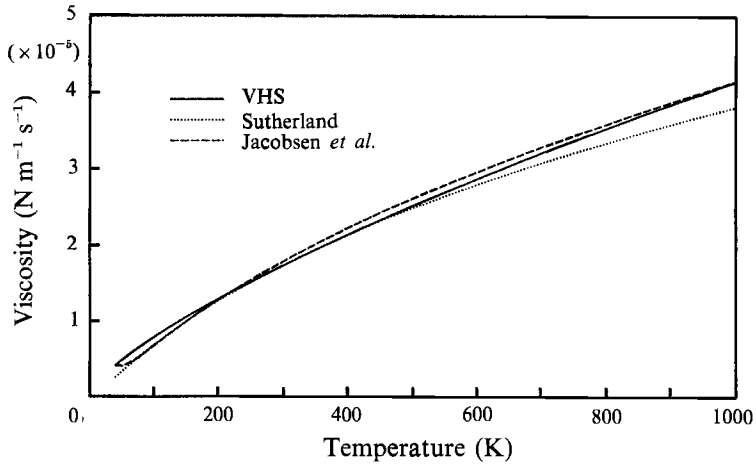

FIGURE 1. Comparison of viscosity models as a function of temperature.

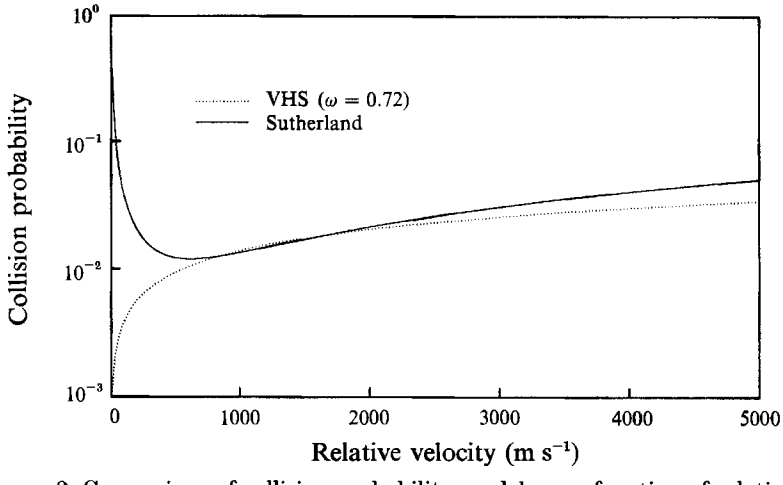

FIGURE 2. Comparison of collision probability models as a function of relative velocity.

where m is the molecular mass. This expression goes to infinity at $g = 0$. In the DSMC simulation, however, the probability of obtaining a relative velocity of zero between two different particles is zero. It should still be noted that large collision cross-sections are obtained with the model for small values of g. When T^* is set to zero in (10), the hard-sphere cross-section is recovered.

For comparison, collision probabilities are shown in figure 2 as a function of relative collision velocity for the VHS and Sutherland potentials for nitrogen. For the VHS model, the value of ω is set to 0.72. In the Sutherland model, a value of $T^* = 91.5$ K is employed which is the value used previously (Boyd 1990) in (5). This value is close to the value of $T^* = 104$ K recommended by Chapman & Cowling (1970) for nitrogen. The appropriate reference collision cross-sections in (2) and (10) have been obtained with a reference viscosity coefficient of 1.63×10^{-5} N m^{-1} s^{-1} at 273 K. The most significant difference between the two models is found at very low collision energies. Here, the attractive part of the Sutherland potential causes the collision probability to increase rapidly. In the VHS model, the probability of collision at low energies approaches zero. The interaction between colliding bodies for the Sutherland potential is again modelled using hard-sphere collision mechanics.

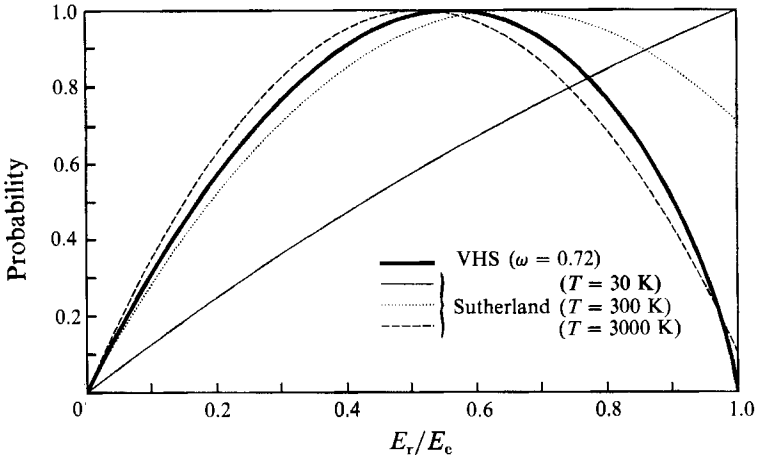

FIGURE 3. Comparison of distributions for the post-collision partitioning of rotational energy.

The mechanics of energy exchange between the rotational and translational modes is again simulated using the Borgnakke–Larsen approach. The distribution function for the translational collision energy filtered by the Sutherland collision cross-section, (10), may be shown to be given by

$$f_{\text{Suth}}\left(\frac{E_t}{kT}\right) = \frac{1}{1+3T^*/T}\left(\frac{E_t}{kT}+\frac{3T^*}{T}\right)\exp\left(\frac{-E_t}{kT}\right). \tag{11}$$

Once again, the hard-sphere result is recovered when the characteristic temperature is set to zero. This distribution is employed together with that for the rotational energy in the collision to obtain the following conditional distribution:

$$f_{\text{Suth}}\left(\frac{E_t}{E_c}\right) = \frac{\zeta^\zeta}{(\zeta-1)^{\zeta-1}}\frac{(E_t/E_c+3kT^*/E_c)\,(1-E_t/E_c)^{\zeta-1}}{1+3kT^*/E_c}. \tag{12}$$

The sampling of the quantity E_t/E_c from (12) is dependent on the value of E_c. This is different from the equivalent VHS distribution, (4). The distribution for the ratio of rotational energy to total collision energy is simply $1-f(E_t/E_c)$. These distributions are shown in figure 3 for three different reference temperatures, and compared to the VHS result for $\omega = 0.72$. The effect of increasing temperature is to move the Sutherland distribution closer to the hard-sphere result, obtained by setting ω equal to 0.5. At the lowest temperature, the Sutherland model provides higher probabilities of obtaining large fractions of rotational energy. Simultaneously, the Sutherland model provides smaller probabilities of obtaining small fractions of rotational energy.

The modelling of the rotational relaxation rate is again performed using Parker's classical result. It may be shown that the distribution for the total collision energy for the Sutherland model is given by

$$f_{\text{Suth}}\left(\frac{E_c}{kT}\right) = \frac{(E_c/kT)^\zeta \exp(-E_c/kT)}{1+3T^*/T}\left[\frac{1}{\Gamma(2+\zeta)}\frac{E_c}{kT}+\frac{1}{\Gamma(1+\zeta)}\frac{3T^*}{T}\right]. \tag{13}$$

Parker's expression consists of three distinct terms each with its own temperature dependence. These are accounted for in the particle simulation probability in the following manner:

$$\phi_{\text{Suth}} = Q_1(E_c)+Q_2(E_c)+Q_3(E_c). \tag{14}$$

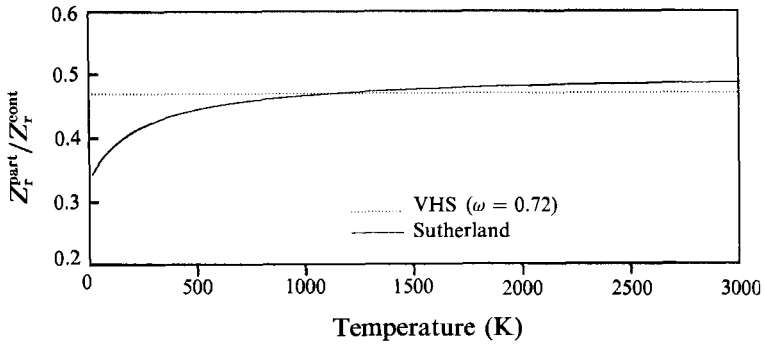

FIGURE 4. Variation with temperature of the correction factor applied to the rotational collision number in the DSMC technique for the two collision models.

It has been assumed that the general form for each of these terms is

$$Q_i(E_c) = \frac{a_i(E_c)^{\alpha_i+1} + b_i(E_c)^{\alpha_i}}{[E_c/\Gamma(2+\zeta)] + [3kT^*/2\Gamma(1+\zeta)]}, \tag{15}$$

where a_i, b_i, and α_i are constants to be determined for each of the three terms in the probability. By integrating (14) over the distribution, (13), and equating with (5) the following results are obtained:

$$a_i = \frac{c_i(kT^*)^{-\alpha_i}}{\Gamma(\alpha_i+2+\zeta)}, \quad b_i = \frac{c_i(kT^*)^{-\alpha_i} 3kT^*}{\Gamma(\alpha_i+1+\zeta)}, \tag{16a, b}$$

where

$$\alpha_1 = 0; \quad c_1 = \frac{1}{Z_\infty}, \quad \alpha_2 = -\tfrac{1}{2}; \quad c_2 = \frac{\pi^{\frac{3}{2}}}{2Z_\infty}, \quad \alpha_3 = -1; \quad c_3 = \frac{\frac{1}{4}\pi^2+2}{Z_\infty}. \tag{17a–c}$$

The correction term applied to the particle collision number to relate it to Parker's result is given by

$$(Z_r^{part})_{Suth} = Z_r^{cont} \frac{2T+3T^*}{2T+3T^*+\zeta(T+3T^*)}. \tag{18}$$

This last result is temperature dependent, and its variation is shown in figure 4. The introduction of a temperature dependence is unfortunate as it cannot be incorporated into the particle simulation. This result illustrates a difficulty in formulating models for particle simulations which were originally developed for continuum methods. For practical use of (18), it is necessary to use a value of temperature which is the average for the problem under study.

Importantly, the hard-sphere expressions obtained with the VHS model are recovered by setting $T^* = 0$ in all of the theory derived for the Sutherland potential. The application of the new rotational relaxation model in a particle simulation under conditions of a heat bath are considered in the next section.

4. Heat-bath relaxation studies

The models described in the previous section have been implemented and tested first in the relatively simple environment of a heat bath. Under conditions of thermal equilibrium, energy exchange between the rotational and translational modes was computed using the distribution given in (12). It was found that equilibrium was

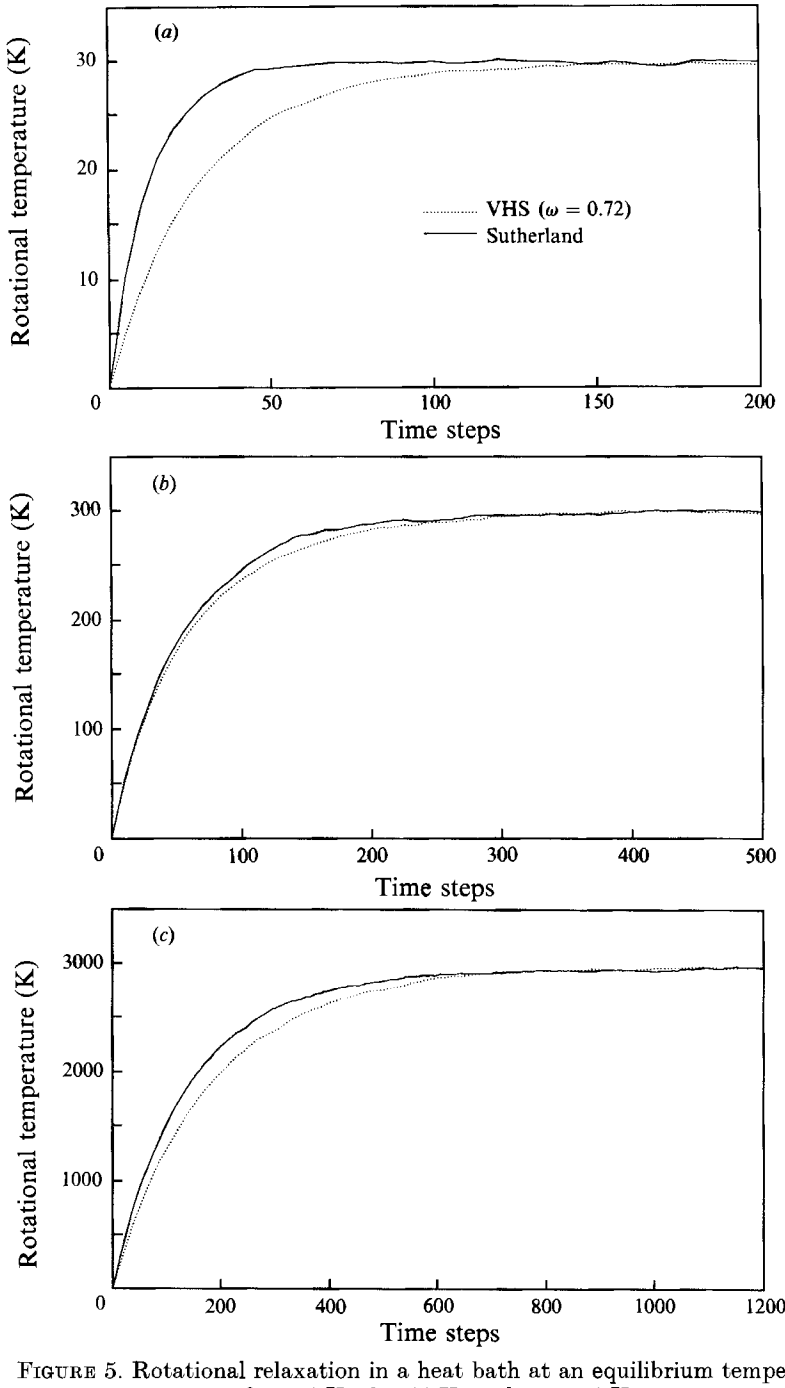

FIGURE 5. Rotational relaxation in a heat bath at an equilibrium temperature of (*a*) 30 K, (*b*) 300 K, and (*c*) 3000 K.

maintained with the new model for simulating rotational relaxation. Similarly, the energy exchange probability given by (14), and corrected by (18), was found to reproduce Parker's formula for equilibrium conditions.

Heat-bath studies were also performed under conditions of thermal non-equilibrium. The particles were initialized with zero rotational energy, and allowed

to relax to a state of equilibrium with the translational modes through collisional energy exchange. The relaxation behaviour computed with the VHS and Sutherland models for three different equilibrium temperatures are shown in figure 5(*a–c*). At the lowest temperature of 30 K, figure 5(*a*), the rate of relaxation simulated with the Sutherland model is much faster than the rate obtained with VHS. This is to be expected from the comparisons of the models shown in figures 2 and 3. At low temperatures, figure 2 shows that the collision rate is greater with the Sutherland potential. Additionally, figure 3 shows that there are larger probabilities of transferring large amounts of energy into the rotational modes following a collision.

In figure 5(*b*) the relaxation profiles for an equilibrium temperature of 300 K are shown. For this case, there is very close agreement between the two models, with the Sutherland model providing a slightly faster relaxation rate. Again, this is the expected behaviour. At temperatures around 300 K, collisions are occurring in the region of figure 2 where there is close correspondence in the collision probabilities. In figure 3 it is shown that there is a small amount of bias towards the transfer of more rotational energy with the Sutherland model at this temperature, which leads to the slightly faster relaxation rate.

Finally, in figure 5(*c*) the relaxation profiles of the models at 3000 K are shown. At this elevated temperature, the relaxation rate obtained with the Sutherland potential has again become larger than the VHS result. This is primarily due to the larger collision probabilities observed in figure 2 for the Sutherland model at large relative velocities. In summary, it is found that the relationship between the two models is not unique, and depends strongly on the temperatures encountered during relaxation.

5. Shock-wave relaxation studies

The first set of experimental measurements considered are those due to Alsmeyer (1976), who employed the electron-beam technique to obtain detailed density profiles in nitrogen over a range of Mach number up to a maximum of about 10. As stated earlier, the experiments were performed in a shock tube, giving a temperature of about 300 K upstream of the shock. From the measured density profiles, Alsmeyer deduced the reciprocal shock thickness. In shock profiles, the lengthscale, x, is often normalized by the upstream mean-free path, λ_1. Flow quantities are normalized in the following way:

$$\bar{y} = (y - y_1)/(y_2 - y_1), \tag{19}$$

where y_1 and y_2 are the upstream and downstream values. When the density, ρ, is normalized by (19), the reciprocal shock thickness is defined as the maximum value of the gradient $\mathrm{d}\bar{\rho}/\mathrm{d}(x/\lambda_1)$. Alsmeyer's data are shown as a function of Mach number in figure 6. Also included are three sets of computations corresponding to three different values for the upstream temperature. The computations were performed with the VHS collision model and the energy-dependent rotational collision number. In (7), T^* is taken to be 91.5 K, and Z_∞ is regarded as a free parameter. For the calculations shown in figure 6 (and in the remainder of this paper) a value of Z_∞ of 18 was employed as this was found to give the best agreement with experiment. While the results are sensitive to Z_∞, this value is only slightly higher than that proposed by Parker (1959) for nitrogen. The calculations are rather less sensitive to the value of T^* employed in the simulations.

At an upstream temperature of 300 K, it is found that very good agreement exists between the numerical and experimental results. The calculations performed for

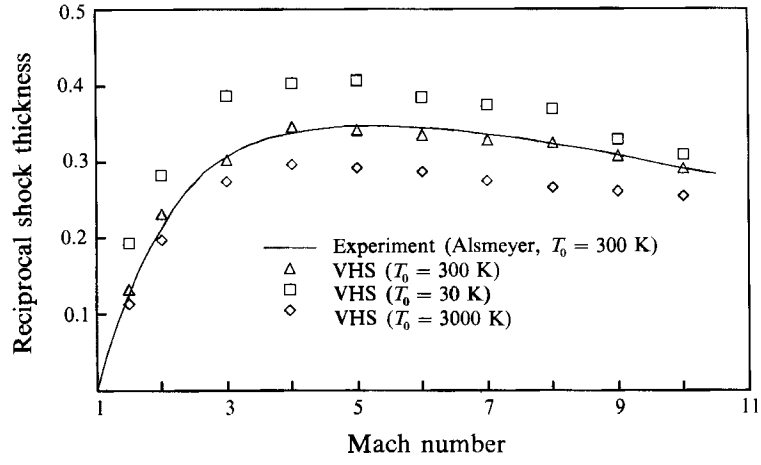

FIGURE 6. Reciprocal shock thickness as a function of Mach number: comparison of Alsmeyer's experiments and VHS computations.

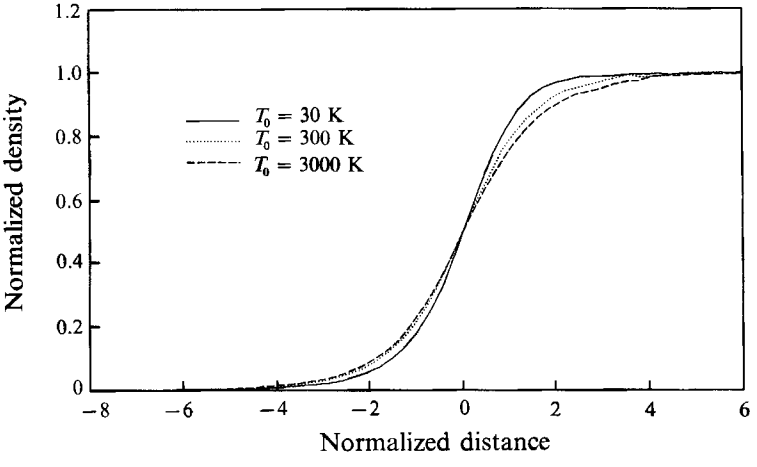

FIGURE 7. Variation with upstream temperature of the density profile computed with the VHS collision model in a Mach 5 shock.

initial temperatures of 30 and 3000 K reveal a strong variation in the shock thickness. At the lower temperature, the reciprocal shock thicknesses are higher, indicating a thinner shock. Conversely, a higher upstream temperature produces thicker shocks. It should be noted that at the elevated upstream temperature of 3000 K, there would be significant vibrational and chemical relaxation in the shock wave. These effects are ignored in the present analysis. The main intent is to understand the variation of rotational relaxation behaviour with temperature.

The density profiles computed at Mach 5 for the three different upstream temperatures are shown in figure 7. The thinning of the shock is clearly discernible as the initial temperature is reduced. The profiles for rotational temperature normalized by (19) are shown in figure 8. The differences between each profile are more exaggerated than those for density. The rotational collision number due to Parker increases with temperature, thereby decreasing the relaxation rate. This behaviour is included in the DSMC computations through (7) and may be observed in figure 9 which shows the variation through the shock wave of the average

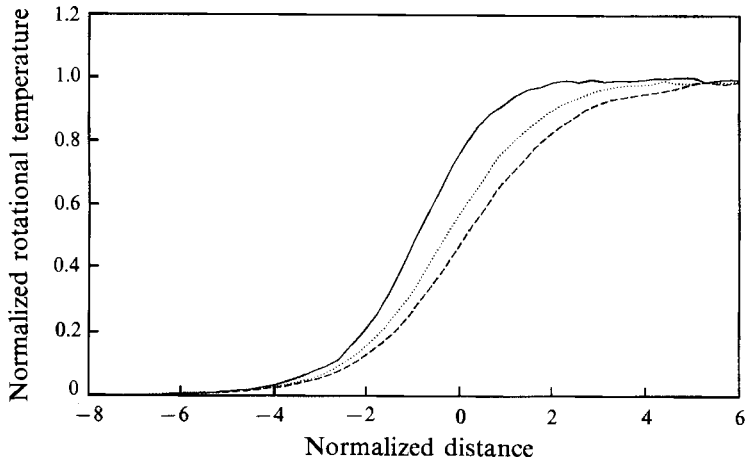

FIGURE 8. Variation with upstream temperature of the rotational temperature profile computed with the VHS collision model in a Mach 5 shock. Curves as for figure 7.

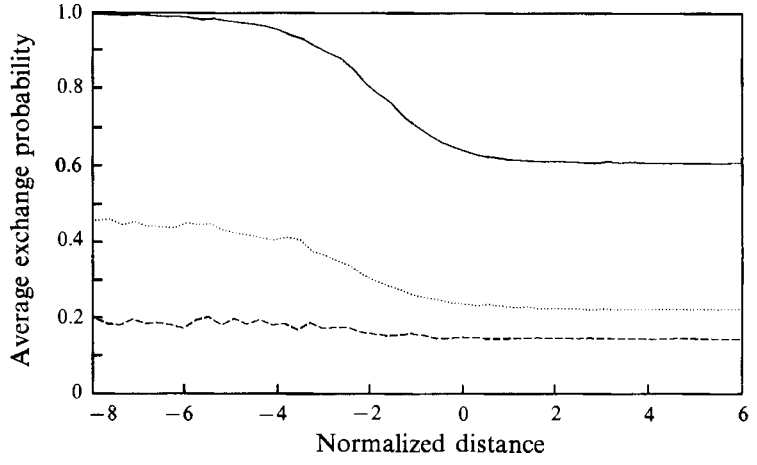

FIGURE 9. Variation with upstream temperature of the profile for the average probability of rotational relaxation computed with the VHS collision model in a Mach shock. Curves as for figure 7.

probability of rotational energy exchange (the reciprocal of the collision number). At the lowest upstream temperature, the relaxation probability is very nearly unity, decreasing down to about 0.6 in the downstream equilibrium region. For this case, the rotational energy mode is equilibrated rapidly. In turn, this phenomenon has the direct effect of producing a thinner shock.

It is interesting to compare the profiles shown in figure 9 with previous DSMC studies which have employed a constant rotational collision number giving a constant exchange probability of 0.2 (Alsmeyer 1976). With an upstream temperature of 3000 K, the variation in the average exchange probability is small and the value is close to 0.2. When the upstream temperature is reduced to 300 K, the average exchange probabilities are increased, although they are still quite close to 0.2. Finally, with the further reduction of upstream temperature to 30 K, a very significant change occurs in the average exchange probabilities. The values are as high as 1 and undergo substantial variation through the shock.

For completeness, the computations discussed above were also performed for a

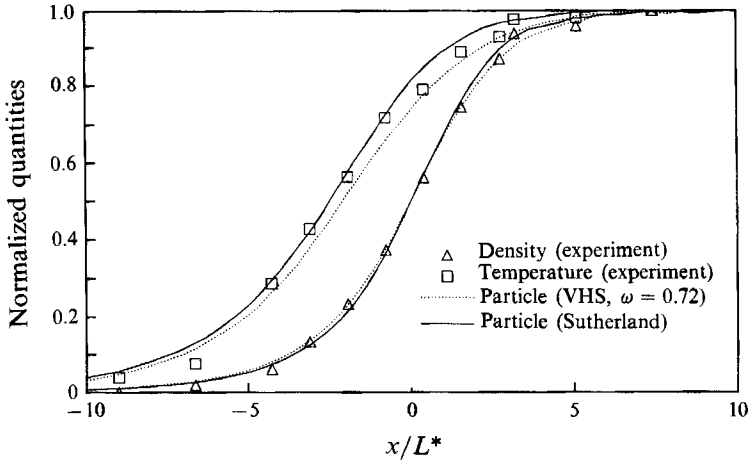

FIGURE 10. Density and rotational temperature profiles for the Mach 7 shock investigated experimentally by Robben & Talbot.

Mach number of 5 assuming a constant energy exchange probability of 0.2 throughout the flow. The computed shock structure obtained for each of the three upstream temperatures considered were identical, when the lengthscale was normalized by the upstream mean-free path, and gave a shock-wave thickness in each case of about 0.322. This illustrates the point that the approach of employing a constant collision number effectively makes the problem non-dimensional.

Computations corresponding to those shown in figure 6 were also performed with the Sutherland collision model. The shock thicknesses calculated at room temperature were in close agreement with the VHS results, as would be expected from figure 5(*b*). At both the lower and higher upstream temperatures, the shocks predicted by the Sutherland model were slightly thinner. This is because the rate of rotational relaxation calculated by the Sutherland model is greater at these temperatures than that obtained with the VHS potential. This behaviour was also anticipated from the heat-bath results given in figures 5(*a*) and 5(*c*). It should be noted that there is a practical difficulty in applying the temperature-dependent correction of (18) in the DSMC calculations. This has been addressed in the present work by employing the average temperature through the shock to evaluate (18) at the beginning of the simulation. This approach will tend to produce a slightly lower collision number in the upstream flow, and a slightly higher collision number in the downstream flow.

Comparison of the experimental data reported by Alsmeyer and Robben & Talbot reveals that the latter measured significantly thinner shocks. Alsmeyer suggested that the difference may be due to non-equilibrium effects in the experiments of Robben & Talbot. The computational results shown in figures 6–9 indicate that the thin shocks observed by Robben & Talbot may be caused by temperature-dependent relaxation effects. It should be noted that the shock thicknesses derived from the experiments of Smith (1972) and Butefisch & Vennemann (1974) tend to agree with the findings of Robben & Talbot. Computations are therefore presented for a number of these experimental investigations which were all characterized by low upstream temperatures.

The electron-beam technique was employed by Robben & Talbot and, in addition to density, the rotational temperature was also measured as shown in figure 10 for a Mach number of 7. Two sets of computations are provided corresponding to the

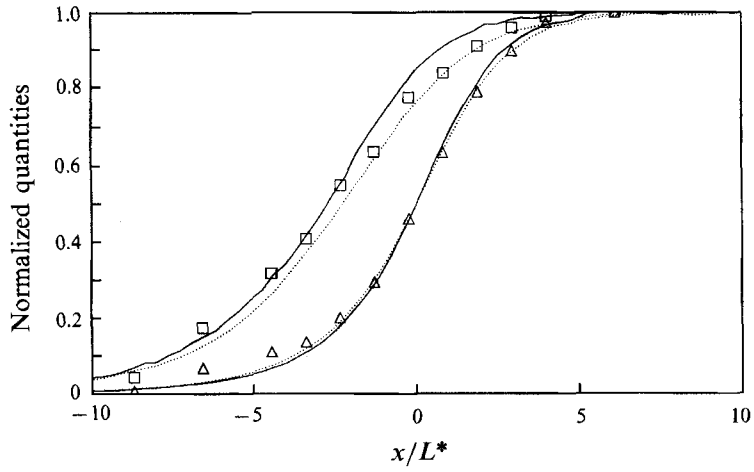

FIGURE 11. Density and rotational temperature profiles for the Mach 12.9 shock investigated experimentally by Robben & Talbot. Symbols as for figure 10.

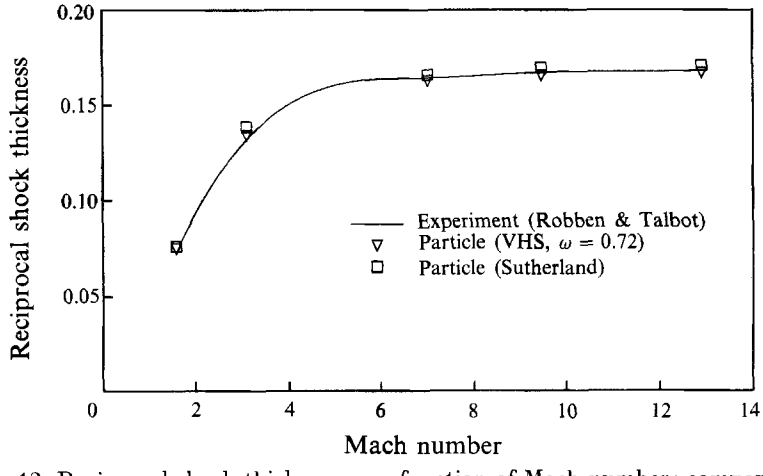

FIGURE 12. Reciprocal shock thickness as a function of Mach number: comparison of Robben & Talbot's experiments and computations.

VHS and Sutherland viscosity laws. The distance through the shock is normalized by the parameter L^* defined by Robben & Talbot as

$$L^* = \mu^*/(\rho u), \tag{20}$$

where μ^* is the viscosity evaluated at the sonic temperature in the shock, and ρu is the mass flux per unit area, which is constant through a shock wave. In the present studies, it has been decided to maintain the normalizing convention of each individual experiment to avoid uncertainties in evaluating a mean-free path at very low temperatures. The values of L^* used to normalize the computational results were taken directly from Robben & Talbot (1966). Figure 10 shows excellent agreement for both numerical solutions and the experimental data. The Sutherland law again gives slightly thinner shock profiles than the VHS model; however, both computations provide an adequate solution of the flow. In figure 11, experimental and numerical profiles are compared at a Mach number of 12.9. Again, very good correspondence between the results is obtained. The computations presented in

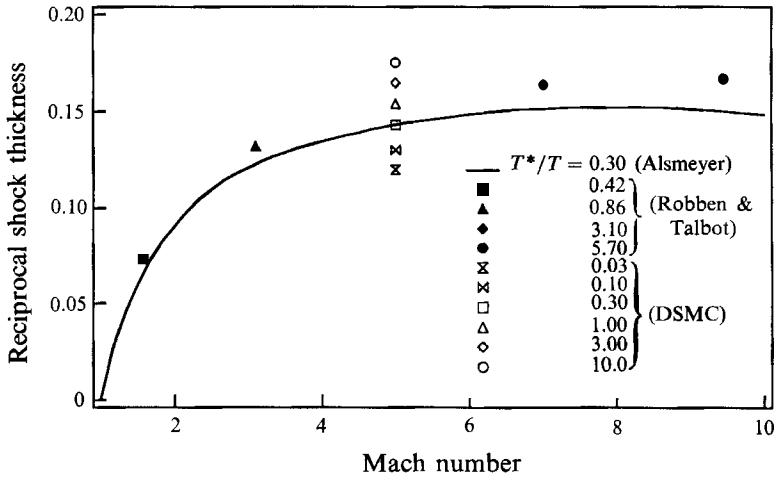

FIGURE 13. Characterization of reciprocal shock thickness using T^*/T_1.

figures 10 and 11 represent the most successful numerical solutions to the experiments of Robben & Talbot following several previous attempts (Alsmeyer 1976; MacPherson 1971; Boyd 1990*a*, *b*).

A comparison of the shock thickness data for these investigations is shown in figure 12 together with the numerical results. The lengthscales have been normalized by the appropriate value of L^*. Additional simulations were performed at Mach numbers of 1.58, 3.1, and 9.45 in order to compare with the full set of data reported by Robben & Talbot. It is found that excellent agreement is obtained over this range of Mach number. All the calculated data lie within the experimental error bounds of 7%.

In addition to Mach number, it is proposed to characterize these shocks in terms of the upstream rotational collision number. One way to do this is to use the ratio of the characteristic temperature for the potential of the molecule, T^*, to the upstream temperature, T_1. For the low-enthalpy facility used by Robben & Talbot the value of T^*/T_1 was as high as 10. In all the experiments of Alsmeyer, T^*/T_1 had a value of about 0.3. The reciprocal shock thicknesses measured by Robben & Talbot, and by Alsmeyer (all based on L^*) are compared as a function of Mach number in figure 13, with the value of T^*/T_1 shown for each case. The shocks measured by Alsmeyer are always thicker than those investigated by Robben & Talbot. However, at the lowest Mach number considered by Robben & Talbot, the value of T^*/T_1 is close to that in the experiments of Alsmeyer, and the shock of Robben & Talbot (which has the lower upstream temperature) is only slightly thinner. As the difference in the value of T^*/T_1 widens for the two experiments, the difference in reciprocal shock thickness increases. This suggests that for each value of T^*/T_1 a curve similar to that shown for Alsmeyer's data may be constructed. As the value of T^*/T_1 is increased, this curve must be moved vertically upwards on figure 13. In this way, each of the data points provided by Robben & Talbot will lie on separate curves corresponding to the relevant value of T^*/T_1. This temperature-dependent behaviour of the shock thickness is predicted by the DSMC technique through use of the energy-dependent exchange probability. A series of simulations were conducted at Mach 5 in which the ratio T^*/T_1 was varied. The results of this investigation are shown as open symbols in figure 13. In agreement with the arguments given above, the reciprocal shock thickness increases significantly as the ratio T^*/T_1 is increased.

Another electron-beam study of rotational relaxation in a shock-wave of nitrogen

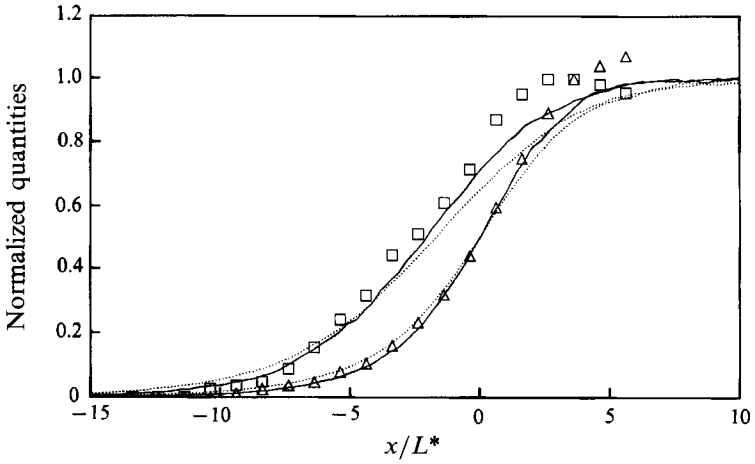

FIGURE 14. Density and rotational temperature profiles for the Mach 26 shock investigated experimentally by Smith. Symbols as for figure 10.

was performed by Smith (1972) who again obtained both density and rotational temperature profiles. In this case, the gas was heated to about 1300 K prior to expansion through a nozzle. In this manner, a Mach number of 26 was obtained. Computations performed with both viscosity models are compared with the experimental data in figure 14. The lengthscale is normalized by the value of L^* provided by Smith. Good agreement is obtained between the computations and the experimental data in the front part of the shock. The very low upstream temperature for this case results in a slightly thinner shock with the Sutherland potential. Unfortunately, Smith reports that the data obtained in the rear portion of the shock were affected significantly by heat transfer between the high-temperature gas and the shockholder. This effect was not included in the computations. However, if the experimental measurements at the front of the shock are reliable, then Smith's data offer further support for the rotational relaxation models employed in this investigation. The current DSMC computations offer improvement over the analysis presented by Smith (1972) in his original paper, particularly in terms of matching the temperature profile.

The final set of experimental data considered is that obtained by Butefisch & Vennemann (1974) who employed an ion time-of-flight technique to measure the velocity profile through a shock. Once again, the gas was preheated, to about 1330 K, and a Mach number of 24 was obtained. The experimental and numerical results are compared in figure 15. Following Butefisch & Vennemann, the lengthscale is normalized by D, the entrance diameter of the shock-holder employed in the experimental investigation. The velocity has been normalized by

$$\bar{u} = (u_2 - u)/(u_2 - u_1). \tag{21}$$

As with the previous comparisons, the numerical results offer excellent agreement with the experimental data. The Sutherland viscosity model gives a slightly thinner shock than the VHS potential. It is believed that this is the first time that a numerical solution has been published for this experiment.

At first sight, because of very low upstream temperatures, it may appear inappropriate to employ the VHS and Sutherland viscosity models for many of the shock waves which have been computed in this study. However, the data shown in

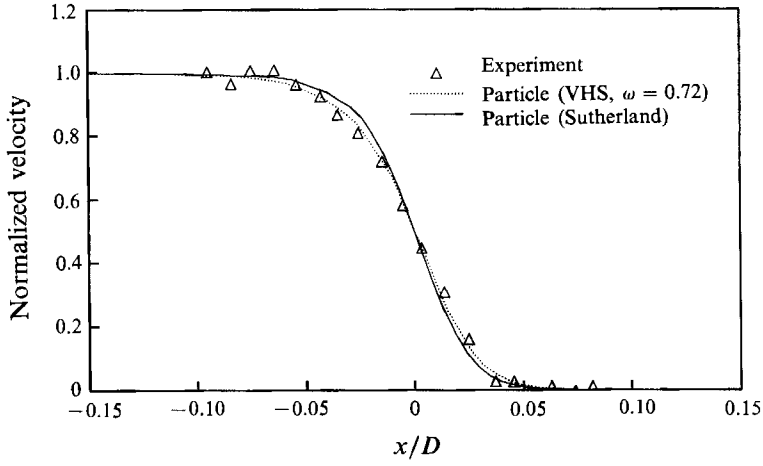

FIGURE 15. Velocity profiles for the Mach 24 shock investigated experimentally by Butefisch & Vennemann.

figure 1 indicate that at 100 K there is only a 16% difference between the VHS viscosity model and the detailed calculations of Jacobsen *et al.* (1973). At the same temperature there is less than 2% difference between the Sutherland model and the result of Jacobsen. By the time the temperature has risen to 200 K the difference is about 1% for both models. For the shock waves investigated in this study, the assumption of employing the VHS and Sutherland models is only inaccurate right at the initial rise in temperature at the front of the shock. However, through most of the shock structure, the temperature is sufficiently high to justify use of these simple models. In terms of shock thickness, it should be noted that the translational temperature rises in advance of the density, so that any small inaccuracies in the temperature profiles do not influence the density profiles to any great extent. The initial rise in temperature at the front of the shocks could be better simulated with the VHS model by determining an appropriate low-temperature value of ω for (1) from figure 1. However, this value would only be valid at the front of the shock, and would be inaccurate in the remainder of the flow. It therefore appears that the VHS model with an exponent of $\omega = 0.72$ is an effective compromise for the flow conditions investigated.

Generally, the results generated in this study indicate that the more sophisticated collision model of Kuscer gives slightly poorer agreement with the experimental data than the simpler VHS model. There are a number of potential explanations for this observed behaviour. This is the first time that results from Kuscer's hard-sphere form of the Sutherland potential have been obtained in the DSMC technique. There is still a requirement for a detailed study to be performed in a monatomic gas to determine whether this model faithfully reproduces the behaviour of the true Sutherland model for collision dynamics. In addition, there is the uncertainty over evaluating the correction term, (18), for the rotational collision number. However, the purpose of the present study was the extension of the Kuscer model for simulating rotational relaxation. In comparison to the experimental data, both the Kuscer and the VHS models give very good agreement, so that each approach may be considered to have been successfully evaluated for the flow conditions examined.

6. Conclusions

An important new finding of the study was that the reciprocal thickness of a normal shock wave, for a rotationally relaxing gas, is dependent on the absolute value of the temperature upstream of the shock. It was proposed that this behaviour be described in terms of the ratio of the characteristic temperature for the potential of the molecule, T^*, to the upstream temperature in the shock, T_1. It was found that as the ratio T^*/T_1 was increased, the shock for a particular Mach number became thinner. The need for characterization of shock waves in terms of T^*/T_1 as well as Mach number is a direct result of the temperature dependence of the rotational collision number. At low temperatures, the rotational collision number is low leading to rapid equilibration and a relatively thin shock. At high temperatures, the rotational collision number is significantly higher resulting in a relatively large relaxation zone and hence a thicker shock. When a constant rotational collision number was employed, the computed shock structure (normalized by the upstream mean free path) was independent of the absolute value of the upstream temperature. This approach has previously failed to account for the differences observed in various experimental data sets which were generated at different upstream temperatures.

A much smaller temperature dependence was also introduced into the calculations through the use of the Sutherland viscosity law instead of the fixed-temperature-exponent VHS law. The Sutherland model gave more rapid relaxation at low and high temperatures, providing slightly thinner shock profiles under such conditions. At room temperature, the two models gave essentially identical results.

Comparisons between a number of different experimental measurements of different flow quantities and the two viscosity models were favourable. Indeed, the computational results reported here represented either the most successful reproductions or the first solutions of the experimental data. These findings indicated that the DSMC technique may be applied with some confidence to such flows provided that the variation in collision number with collision energy is accounted for. This is a significant result as many experimental facilities for investigating non-equilibrium phenomena in normal shock waves still rely on low-enthalpy conditions.

The theory developed for the use of the Sutherland model indicated that more sophisticated intermolecular potentials may be employed in the DSMC technique. Similar theoretical developments may also be derived for the simulation of vibrational and chemical relaxation. In this regard, it is noted that G. A. Bird (1991, personal communication) has combined the VHS and Sutherland potentials into a general model. The expressions derived in this paper for the Sutherland model may be generalized to Bird's new model, although it is not expected that this will alter the results reported here to any significant extent.

Support for the author was provided by NASA (Grant NCC2-582).

REFERENCES

ALSMEYER, H. 1976 Density profiles in argon and nitrogen shock waves measured by absorption of an electron beam. *J. Fluid Mech.* **74**, 497–513.

BIRD, G. A. 1976 *Molecular Gas Dynamics*. Clarendon.

BIRD, G. A. 1981 Monte Carlo simulation in an engineering context. In *Rarefied Gas Dynamics*, Part 1, pp. 239–255. AIAA.

BORGNAKKE, C. & LARSEN, P. S. 1975 Statistical collision model for Monte Carlo simulation of polyatomic gas mixtures. *J. Comput. Phys.* **18**, 405–420.

Boyd, I. D. 1990*a* Rotational–translational energy transfer in rarefied nonequilibrium flows. *Phys. Fluids* A **2**, 447–452.

Boyd, I. D. 1990*b* Analysis of rotational nonequilibrium in standing shock waves of nitrogen. *AIAA J.* **28**, 1997–1999.

Boyd, I. D. 1992 Analysis of vibration-dissociation-recombination processes behind strong shock waves of nitrogen. *Phys. Fluids* A **4**, 178–185.

Brau, C. A. & Jonkman, R. M. 1970 Classical theory of rotational relaxation in diatomic gases. *J. Chem. Phys.* **52**, 477–484.

Butefisch, K. A. & Vennemann, D. 1974 Absolute velocity measurements in a rarefied gas flow by an ion time-of-flight technique. In *Rarefied Gas Dynamics*, pp. 245–252. Academic.

Chapman, S. & Cowling, T. G. 1970 *The Mathematical Theory of Non-Uniform Gases*. Cambridge University Press.

Jacobsen, R. T., Stewart, R. B., McCarty, R. D. & Hanley, H. J. M. 1973 Thermophysical properties of nitrogen. *Natl Bureau Stand. Tech. Note* **648**, 11–15.

Kuscer, I. 1989 A model for rotational energy exchange in polyatomic gases. *Physica* A **158**, 784–800.

Lumpkin, F. E., Haas, B. L. & Boyd, I. D. 1991 Resolution of differences between collision number definitions in particle and continuum simulations. *Phys. Fluids* A **3**, 2282–2284.

MacPherson, A. K. 1971 Rotational temperature profiles of shock waves in diatomic gases. *J. Fluid Mech.* **49**, 337–351.

Melville, W. K. 1972 The use of the loaded-sphere molecular model for computer simulation of diatomic gases. *J. Fluid Mech.* **51**, 571–583.

Parker, J. G. 1959 Rotational and vibrational relaxation in diatomic gases. *Phys. Fluids* **2**, 449–462.

Robben, F. & Talbot, L. 1966 Measurement of shock wave thickness by the electron beam fluorescence method. *Phys. Fluids* **9**, 633–662.

Smith, R. B. 1972 Electron-beam investigation of a hypersonic shock wave in nitrogen. *Phys. Fluids* **15**, 1010–1017.